Design of All Dielectric Frequency Selective Surfaces

Design of All Dielectric Frequency Selective Surfaces

Andrei-Marius Silaghi
Dept. of Measurements and Optical Electronics
University Politehnica Timisoara
Timisoara, Romania
andrei.silaghi@upt.ro

Aldo De Sabata
Dept. of Measurements and Optical Electronics
University Politehnica Timisoara
Timisoara, Romania
aldo.de-sabata@upt.ro

Ladislau Matekovits
Dept. of Electronics and Telecommunications
Politecnico di Torino
Torino, Italy
ladislau.matekovits@polito.it

***Abstract*—Several all-dielectric surfaces are introduced in this paper aiming to obtain various stop bands between 6 and 12 GHz, and also demonstrating that filtering in the X band (8-12 GHz) can be achieved without the use of metallic structures. Properties of the structures have been assessed by full-wave simulation. The parametric analyses included in the research also showed that changing the geometrical parameters enabled the control of the working frequency. The performance of the proposed structures has been assessed through the reflection coefficient, whilst also dielectric resonator theory (interpretation of effective permittivity and permeability) has been approached to explain the operation of the proposed structures.**

Keywords—all dielectric, Frequency Selective Surface, dielectric resonator, stop band, X band.

I. INTRODUCTION

Frequency selective surfaces (FSSs) are 2D periodic dielectric or metallic-dielectric structures that are used to control propagation of incident electromagnetic waves [1].

Lately, engineering professionals have been paying considerable attention to FSSs, initially because of their use in devices like reflectors, selective absorbers, and spatial filters. A dielectric substrate carries the imprint of a periodic metal pattern, often a cost-effective one like FR4, to create the simplest practical implementation of FSSs [2].

If we discuss in terms of material types, the use of dielectric materials rather than metallic designs can produce a more functional design for an FSS. Additionally, depending on their thermal, electrical or mechanical characteristics, FSSs built of dielectric materials can be employed in a variety of harsh conditions [3].

Fabrication techniques to build and experimental validate dielectric samples are presented in [4] and [5]. For example, in [4] stereolithography is used for 3D printing technology, whilst in [5] additive manufacturing is performed to fabricate an all-dielectric sample.

Various applications can be found for these types of FSSs. Firstly, a mechanically tunable FSS based on a sliding inserted dielectric is proposed in [6]. Next, in [7] an all-dielectric frequency-selective surface for high power microwaves was created (arcing at field concentration locations and heating in the conductors were prevented by not using metals). Furthermore, a periodic stack of isotropic dielectric substrates exhibiting birefringence makes up a proposed converter in [8]. Moreover, in [9] a Y-shaped barium strontium titanate ceramic resonator-based all-dielectric metamaterial FSS is introduced and explained.

Together with the evaluation of the employed materials, the subject of designing all dielectric FSSs has been tackled in the literature [6], [10]-[12].

First, a mechanically tunable FSS based on a sliding inserted dielectric is tackled in [6]. The tunable FSSs operating mechanism is first described in this research, and it suggests that the changeable capacitance is the key to tunability. Based on this, the authors create an all-metal bandpass FSS with a specific thickness and an insert dielectric with a matching cross shape. The dielectrics insertion depth can be changed to alter the resonance frequency. A better a construction with a tripole hole and a hollow support is suggested to increase performance. The simulation yields a tunable range of 3.24 to 5.52 GHz and high angular stability [6].

For X-band applications, it is suggested in [10] to design an all-dielectric band-stop FSS. The proposed configuration consists of a planar array of ceramic hexagonal prisms with a honeycomb-like topology. Three resonant dips are present in the proposed FSS.

The dips are combined to create a broad stop-band with a -10-dB fractional bandwidth of 24.4% (central frequency of 10 GHz). The cylindrical cavity mode analysis based on the cylindrical wave functions is used to illustrate resonant characteristic modes [10].

In [11], the authors use dielectric ceramics to create a band-stop all-dielectric metamaterial FSS. To create the desired forms, four rectangular ceramic blocks that have high permittivity and low dielectric loss have been joined together. According to the reported simulation results, the FSS can reach a stop band in the range of 6.97 to 8.85 GHz, this response being affected by parameters such as: the dielectric unit cells geometrical structure or the permittivity of the dielectric material [11].

Next, the study from [12] presents the design of a narrow, high-efficiency pass-band all-dielectric metamaterial FSS. The pass band operates between 8.92 GHz and 9.16 GHz. In order to analyze the FSS, the effective permittivity, effective permeability, and normalized impedance are extracted, and the electric and magnetic fields are monitored [12].

The outcome demonstrates that the resonance modes and impedance match of the all-dielectric metamaterial FSS may be modified to create a custom metamaterial. This type of FSS is capable of exhibiting the not only the characteristics that metallic FSSs have but also the benefits of all-dielectric materials, such as high-power handling capabilities or high temperature [12].

In this paper, we propose some structures of all-dielectric FSSs made of ceramic. The proposed solutions are investigated by usual means in relation to FSSs (calculation of transmissions coefficient and parametric variation of angle of incidence) and also by means related to dielectric resonators. Effective permittivity and permeability are extracted in order to demonstrate the functionality of the proposed FSSs. Also, surface currents are plotted at different frequencies. By modifying geometrical parameters, and extra-large stopband is obtained.

The paper is organized as follows. In Section II, the theory of operation of dielectric FSSs is presented (Mie and dielectric resonator theory). The design of several all-dielectric FSSs is presented, and its filtering properties are assessed in Section III. It is shown how the modification of geometrical parameters impact the occurrence and position of different stopbands in the frequency domain. The last section is dedicated to conclusions.

II. Theory of Operation

The composite medium can be used as a metamaterial by adding high-permittivity, sub-wavelength "atoms" of dielectric materials to the low-permittivity matrix [3].

The Nicholson-Ross-Weir approach can be used to derive effective relative permittivity and permeability from S parameters, which can then be used to explain the macroscopic electromagnetic response. Dielectric materials are used as sub-wavelength dielectric resonators in this instance, [3].

The dielectric resonator theory states that, by adjusting geometrical shapes, geometrical dimensions, and relative permittivity, various resonant modes are launched at intended frequencies. At specific frequencies, different dielectric resonators can generate a variety of resonant modes. Effective relative permittivity and permeability values can be adjusted at will due to the capacity to tune resonant modes [3].

A. Mie theory

The resonant wavelengths inside the dielectric inclusions of the order of to the diameters of the inclusions, however the wavelengths outside the inclusions are greater than the sizes of the inclusions if the permittivity of the inclusions is significantly greater than that of the background matrix. The effective medium hypothesis can be used to characterize the combination under these circumstances [3].

B. Dielectric resonator theory

At matching frequencies, a dielectric structure of the right size can be viewed as a dielectric cavity. This equivalence becomes more realistic in the case of materials with large permittivities, due to the magnetic wall that acts as boundary condition for high permittivity dielectrics. In the dielectric cavity, the incident wave is backwards and forward reflected, creating a stationary wave and acting as a dielectric resonator [3].

III. Simulation Results

A. Initial simulations

Figure 1 shows the geometry of our first proposed all-dielectric FSS. The structure has a unit cell with sizes of d_x=10 mm and d_y=10 mm. It consists of a cylinder having an outer radius of 3 mm and an inner radius of 2 mm, made entirely of dielectric. The height of the cylinder is 3.2 mm, and the chosen material was ceramic having: ε_r=110 and μ_r=1 (non-magnetic material), tan (δ)=0.0015.

Rectangular ceramic blocks with these dimensions and relative permittivity, can be used as dielectric resonators. Utilizing the CST Microwave Studios [13] frequency-domain solver, which applies unit cell (periodic) boundary conditions to the four boundaries along the x and y axes, the electromagnetic response to incident plane waves has been simulated. Our goal was to construct an all-dielectric filter for the X band (8–12 GHz), which is frequently utilized in automotive area.

In Fig. 2, the magnitude of the transmission coefficient S_{21} of a linearly polarized plane wave in normal incidence is reported between 1 and 11 GHz (TE case). We can notice a notch centered at 8.41 GHz, with -10 dB stop band between 8.33 and 8.51 GHz.

A parametric investigation on the structure in Fig. 1 has been carried out to evaluate the sensitivity in relation to the electromagnetic plane waves incidence angle. Only the change of the transmission coefficient with the colatitude angle has been taken into account due to the symmetry of the structure [2]. Results of the parametric modification of theta (colatitude angle) are shown in Fig. 3. This setting has been changed five times, from 0 to 60 degrees.

By performing a parametric variation of theta between 0 and 60 degrees, in steps of 15 degrees, an interesting behavior can be observed. Firstly, the notch is slightly shifted to lower frequencies from 8.41 to 8.36 GHz.

Secondly, a new notch appears at lower frequency. For example, for θ=60°, the second notch occurs at 6.13 GHz. The same parametric study has been undergone for the TM case, being reported in Fig. 4. Again, a second notch appears for the same range of incidence angles theta as in the TE.

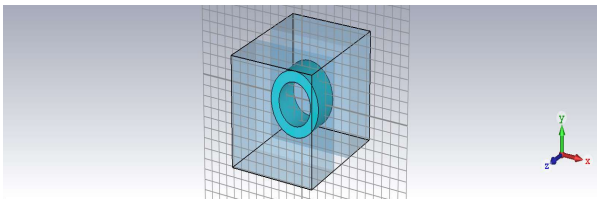

Fig. 1. Geometry of the first proposed dielectric structure (unit cell).

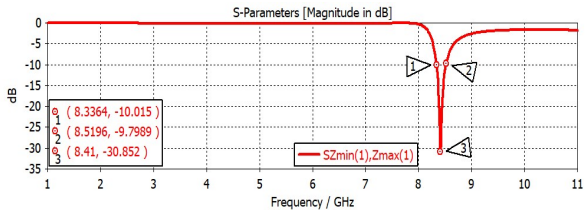

Fig. 2. Transmittance coefficient for the structure in Fig. 1.

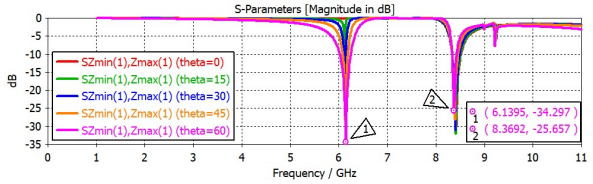

Fig. 3. Parametric variation of the incident angle theta for the structure in Fig. 1 (TE Mode).

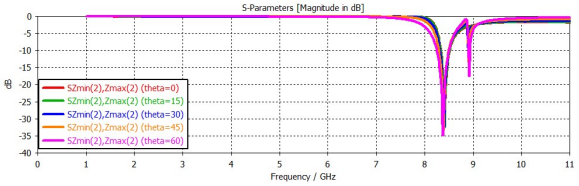

Fig. 4. Parametric variation of the incident angle theta for the structure in Fig. 1 (TM Mode).

In order to explain the above-reported results, we switched to using the dielectric resonator theory. With the *S* parameters obtained from the simulation, we performed a postprocessing task, namely extracting the effective permittivity and permeability (from Template Based Post-Processing - General Results - S Parameters - Extract Permittivity and Permeability from S-Parameters).

Figure 5 and Fig. 6 present the above-mentioned results and can be used to explain the reason why we encounter impedance match or mismatch. They show that a magnetic resonance happens at about 8 GHz (Fig. 6). The effective permeability reaches its positive maximum and then becomes negative, indicating a diamagnetic behavior of the material. At 8.8 GHz, the permittivity (Fig. 5) reaches its positive maximum and then becomes negative. The resonances of permittivity and permeability are separated from one another in the frequency range under consideration. So the effective impedance of the structure is mismatched with respect to the impedance of the surrounding medium, and the stop band occurs (from Fig. 2, between 8 and 8.8 GHz).

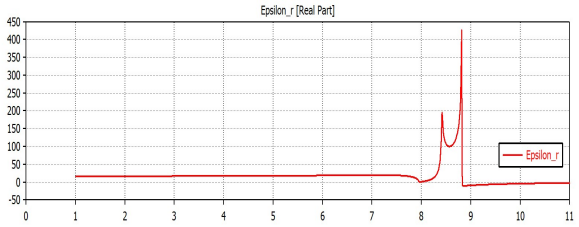

Fig. 5. The effective permittivity for the structure in Fig. 1.

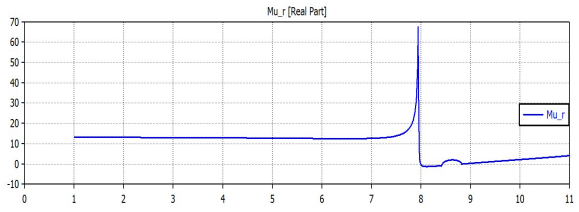

Fig. 6. The effective permeability for the structure in Fig. 1.

Moreover, in order to better explain the functionality of the proposed structure, surface currents have been obtained by simulation. Figure 7 shows the surface currents outside the stopband (at 6 GHz). These currents have small values (up to 12 A/m). In Fig. 8, surface currents at 8.41 GHz are reported. The results support the theory concerning the occurrence of the stop band (larger values of the surface current, up to 50 A/m are present).

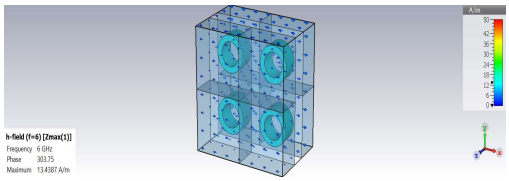

Fig. 7. Surface currents at 6 GHz.

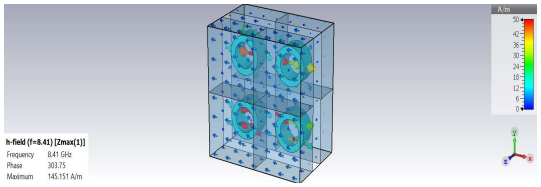

Fig. 8. Surface currents at 8.41 GHz.

B. *Other scenarios*

Next, other scenarios have been investigated. Firstly, we performed a geometrical modification on the structure from Fig. 1. In Fig. 9, one can observe the new dielectric structure, having this time an outer radius of 4.5 mm and inner one of 3.5mm (thus an increase of 1.5 mm for both radii). Again, the structure is all-dielectric, the material being ceramic: ε_r=110, μ_r=1, tan (δ)=0.0015, having the same sizes for the unit cell, and the same height (3.2mm).

The simulated transmittance for this FSS is visible in Fig. 10. It shows and enhanced result, by the presence of two wide stopbands: one appears between 8.16 GHz and 8.63 GHz and another larger one between 9 and 11.74 GHz.

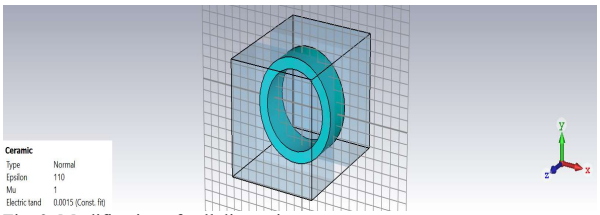

Fig. 9. Modification of cell dimensions.

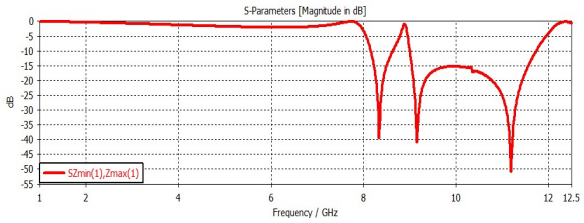

Fig. 10. Result for Fig.9 in TE incidence.

Furthermore, a different geometrical modification was to place another small cylinder inside the outer one (see Fig. 11), so making a combination between the unit cell structures in Fig. 1 and Fig. 9.

The outer ring has the same dimensions as the one reported in Fig. 9 (4.5 mm outer radius and inner radius of 3.5 mm), whilst the inner circle has the dimensions from Fig. 1 (3 mm-outer radius and 2 mm-inner radius). The unit cell dimensions are not changed, both of them being 10 mm, and the height of the cylinders remaining 3.2 mm.

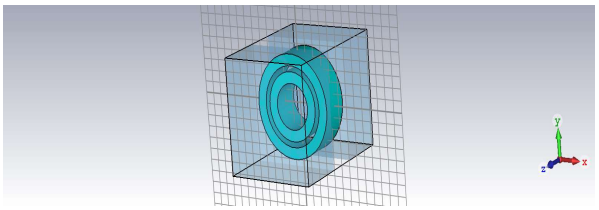

Fig. 11. Two dielectric cylinders.

This time, the results from Fig. 12 show that another method to obtain a second stop band has been devised. A shift in frequency occurs with 2 cylinders present: the first stop band is this time between 7.11 and 7.92 GHz, whilst the second one appears between 8,3 and 10.12 GHz.

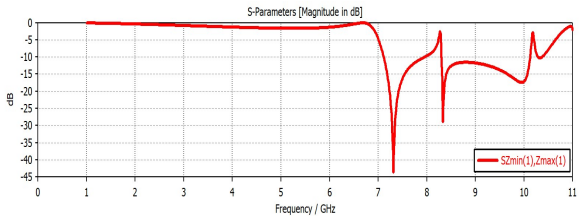

Fig. 12. Reflection coefficient for normal incidence for the structure in Fig.11.

IV. Conclusions

In this study, we have introduced some all dielectric FSS structures in order to obtain spatial filtering in the X band (8-12 GHz). The stop bands have been obtained without the use of metallic components.

A short literature review has been undergone to present multiple applications of all dielectric structures. The dielectric resonator theory has been also shortly revised.

Several structures have been introduced: one relying on a unit cell containing a dielectric hollow cylinder one containing two dielectric cylinders. Parametric studies have been performed and reported.

Results have been presented in terms of usual FSS evaluation items (such as transmission coefficient and parametric variation of different colatitude angles) and also in terms of dielectric resonator theory (extraction of effective permeability and permittivity, and calculation of surface currents to sustain results obtained by assessment of response to wave incidence).

Results have demonstrated that one stop band (6.1 or 8.4 GHz) or a wide-stop band between 9 and 11.7 GHz can be obtained. In the second case, the X band has been covered.

Acknowledgment

This work was supported by a grant of the Ministry of Research, Innovation and Digitization, CNCS - UEFISCDI, project number PN-III-P1-1.1-PD-2021-0010, within PNCDI III.

References

[1] B. A. Munk, Frequency Selective Surfaces: Theory and Design, NJ: Wiley, 2000.

[2] A. Buta, A. Silaghi, A. De Sabata, L. Matekovits, “Multiple-Notch Frequency Selective Surface for Automotive Applications”, 2020 13th International Conference on Communications (COMM), 18-20 June 2020, Bucharest, Romania, 2020.

[3] J. Wang, S. Qu, L. Li, J. Wang, M. Feng, H. Ma, H. Du, Z. Xu, “All-dielectric metamaterial frequency selective surface”, Journal of Advanced Dielectrics, Vol. 7, Nr. 5 (2017), 1730002-1--1730002-11, 2017.

[4] J. Barton, C. Garcia, E. Berry, R. Salas, R. Rumpf, “3-D Printed All-Dielectric Frequency Selective Surface With Large Bandwidth and Field of View”, IEEE Transactions on Antennas and Propagation, Vol. 63, Nr. 3, March 2015.

[5] R. Mellita, S. Karthikeyan, P. Damodharan, “Additively Manufactured Conformal All-dielectric Frequency Selective Surface”, 2020 50th European Microwave Conference (EuMC), 12-14 January 2021, Utrecht, Netherlands, 2021.

[6] S. Qiu, Q. Guo, Z. Li, “Tunable Frequency Selective Surface Based on a Sliding 3D-Printed Inserted Dielectric”, IEEE Access, Vol. 9, pp. 19743-19748, 25 January 2021.

[7] J. Barton, C. Garcia, E. Berry, R. May, T. Gray, R. Rumpf, “All-Dielectric Frequency Selective Surface for High Power Microwaves”, IEEE Transactions on Antennas and Propagation, Vol. 62, Nr. 7, July 2014.

[8] M. Crespo, G. Ballesteros, G. Goussetis, C. Segura, “Experimental Validation of All-Dielectric mm-Wave Polarization Conversion Based on Form Birefringence”, IEEE Microwave and Wireless Components Letters, Vol. 26, Nr. 10, October 2016.

[9] J. Zhang, Y. Fan, H. Sun, Y. Sun, X. Fan, H. Li, “All dielectric metamaterial frequency selective surface based on Y shaped barium strontium titanate ceramic resonator”, 2019 12th UK-Europe-China Workshop on Millimeter Waves and Terahertz Technologies (UCMMT), 20-22 August 2019, London, United Kingdom, 2019.

[10] J. Tak, J. Choi, “Design of an All-dielectric Band-stop Frequency Selective Surface”, 2016 International Symposium on Antennas and Propagation (ISAP), 24-28 Oct. 2016, Okinawa, Japan, 2016.

[11] L. Li, J. Wang, J. Wang, H. Ma, M. Feng, M. Yan, J. Zhang, S. Qu, “Toward band-stop all-dielectric metamaterial frequency selective surface via dielectric ceramic blocks”, 2016 IEEE MTT-S International Microwave Workshop Series on Advanced Materials and Processes for RF and THz Applications (IMWS-AMP), 20-22 Julyl 2016, Chengdu, China, 2016.

[12] L. Li, M. Feng, J. Wang, J. Wang, H. Ma, J. Zhang, S. Qu, “Design of Narrow Pass-band All-dielectric Metamaterial Frequency Selective Surface”, 2019 IEEE MTT-S International Wireless Symposium (IWS), 19-22 May 20291, Guangzhou, China, 2019.

[13] CST Microwave Studio, v. 2022